2018

pH-Dependent Silica Nanoparticle Dissolution and 1 Cargo Release

Giorgia Giovaninni
Medway School of Pharmacy, Chatham, United Kingdom

Colin J. Moore
Technological University Dublin, FOCAS Research Institute, Dublin, Ireland

Andrew John Hall
University of Kent, Canterbury, United Kingdom

Hugh Byrne
Technological University Dublin, hugh.byrne@tudublin.ie

Vladimir Gubala
Medway School of Pharmacy, Chatham, United Kingdom

Recommended Citation

Giovannini, G., Moore, C.J. & Hall, A.J. (2018). pH-Dependent Silica Nanoparticle Dissolution and 1 Cargo Release. *Colloids and Surfaces B: Biointerfaces*, vol. 169, 1 September 2018, pg. 242-248. doi:10.1016/j.colsurfb.2018.04.064

pH-Dependent Silica Nanoparticle Dissolution and Cargo Release

Giorgia Giovaninni,[a] Colin J. Moore,[b¥*] Andrew J. Hall, [a] Hugh J. Byrne,[b] Vladimir Gubala [a]

[a]Medway School of Pharmacy, University of Kent, Central Ave, Chatham Maritime, Kent, ME4 4TB, United Kingdom

[b]FOCAS Research Institute, Dublin Institute of Technology, Kevin St., Dublin 8, Ireland

Email: gg238@kent.ac.uk, colin.moore@dit.ie, a.hall@kent.ac.uk, hugh.byrne@dit.ie, v.gubala@kent.ac.uk

[¥]Current address: Nanomedicine and Nanoprobes, Faculty of Pharmacy, Université de Tours, 31 Avenue Monge, Tours, 32000, France

*Corresponding author: colin.moore@dit.ie , Tel: +353 1 4027902 , Fax: +353 1 4027901

Abstract

The dissolution of microporous silica nanoparticles (NP) in aqueous environments of different biologically relevant pH was studied in order to assess their potential as drug delivery vehicles. Silica NPs, loaded with fluorescein, were prepared using different organosilane precursors (tetraethoxysilane, ethyl triethoxysilane or a 1:1 molar ratio of both) and NP dissolution was evaluated in aqueous conditions at pH 4, pH 6 and pH 7.4. These conditions correspond to the acidity of the intracellular environment (late endosome, early endosome, cytosol respectively) and gastrointestinal tract ('fed' stomach, duodenum and jejunum respectively). All NPs degraded at pH 6 and pH 7.4, while no dissolution was observed at pH 4. NP dissolution could be clearly visualised as mesoporous hollows and surface defects using electron microscopy, and was supported by UV-Vis, fluorimetry and DLS data. The dissolution profiles of the NPs are particularly suited to the requirements of oral drug delivery, whereby NPs must resist degradation in the harsh acidic conditions of the stomach (pH 4), but dissolve and release their cargo in the small intestine (pH 6 - 7.4). Particle cores made solely of ethyl triethoxysilane exhibited a 'burst release' of encapsulated fluorescein at pH 6 and pH 7.4, whereas NPs synthesised with tetraethoxysilane released fluorescein in a more sustained fashion. Thus, by varying the organosilane precursor used in NP formation, it is possible to modify particle dissolution rates and tune the release profile of encapsulated fluorescein. The flexible synthesis afforded by silica NPs to achieve pH-responsive dissolution therefore makes this class of nanomaterial an adaptable platform that may be well suited to oral delivery applications.

Graphical Abstract

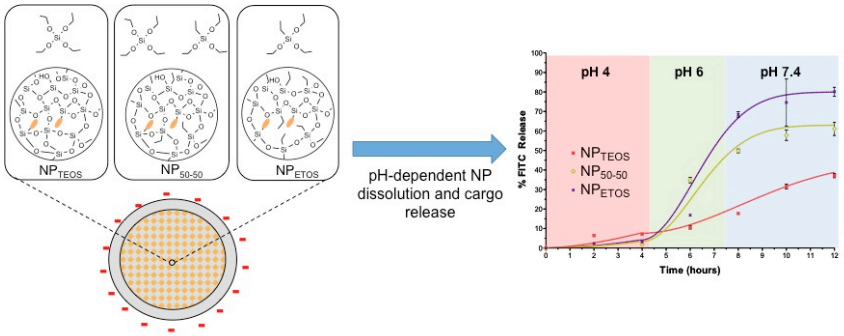

Introduction

Nanoparticle (NP)-based delivery systems have come to prominence over the past two decades as they can be designed to carry poorly soluble drugs or molecules that are prone to degradation in biological conditions.[1-4] NPs can also transport therapeutics across highly regulated biological boundaries such as the blood brain barrier.[5,6] In particular, silica NPs (SiNPs) are regularly described as excellent candidates for drug delivery applications because they are regarded as biocompatible[7-9] and inert.[10] However, it is the adaptable and flexible nature of siloxane chemistry that makes this class of nanomaterial so widely studied as a drug delivery agent. This is facilitated, in part, by the large number of commercially available organosiloxane derivatives that can be used as precursors for SiNP synthesis. The chemistries of these precursors can vary widely and means that SiNPs can exhibit a range of useful physicochemical properties (e.g. different porosity, charge, hydrophobicity), which, in turn, allows for different kinds of therapeutics to be encapsulated and delivered to disease sites.

Most silica-based drug delivery studies employ mesoporous silica, having pore sizes of the order 2-50nm, and rely on tunable cargo release via a 'gatekeeper' strategy.[8,11-14] Despite their popularity, the requirement to load cargo and incorporate gatekeepers after NP synthesis introduces additional complexity to particle design. On the other hand, microporous silica NPs have characteristic pores of less than 2nm[15], that are challenging to characterise accurately with appropriate methods and expertise compared to mesoporous silica.[16] Encapsulatation of different therapeutics can be achieved during NP synthesis [2,17,18] and the release mechanism is via the natural degradation of the silica.[19] The process of NP degradation is therefore largely governed by the organosiloxane precursors, and their associated physicochemical properties, that can be easily imparted during synthesis. However, microporous silica remains understudied as a drug delivery candidate and is more frequently reported in immunoassays[20-22] and bioimaging.[9,23-25] This is surprising, considering the adaptable nature of silica and the fact that it, in comparison to its mesoporous counterpart, avoids the need for gatekeeping to control drug release and the associated complications related to cargo leeching. We therefore feel microporous silica NPs are

an interesting nanomaterial to study and have the potential to impact the drug delivery

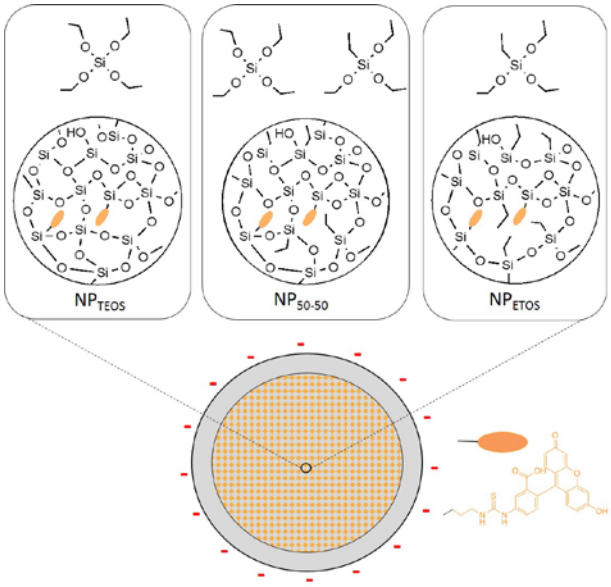

Figure 1: Silica NPs were prepared with different core chemistries by employing different NP precursors during synthesis: tetraethoxysilane (TEOS) or ethyl triethoxysilane (ETOS). These NPs were called NP_{TEOS} and NP_{ETOS}. TEOS and ETOS were also added in an equal molar ratio ($NP_{50\text{-}50}$). Covalently binding fluorescein (FITC) in the NP cores also provided information about particle degradation and cargo release.

field.

We hypothesise the development of a dissolution-based method of controllably releasing encapsulated cargo from microporous SiNPs by synthesising colloids using different organosiloxane precursors. SiNPs are formed utilising hydrolysis but this pH-dependent mechanism is reversible and suggests SiNPs may degrade at different rates in different acidic conditions.

Intracellular NP-drug delivery typically requires endocytosis of the nanocarrier to transport a therapeutic across the cell membrane. Trafficking of the NPs from the extracellular environment (pH 7.4) into early endosomes (pH 6) and then to late endosomes/lysosomes (pH 4) means environments of different acidity are experienced. The same can be said for oral drug delivery applications in which medicines first encounter the harsh environment of the stomach (pH 4 in 'fed state') and are then passed to the duodenum (pH 6) and jejunum (pH 7.4) for adsorption.

We have synthesised core-shell SiNPs via the reverse microemulsion method (Figure 1) and investigated their dissolution in aqueous conditions at biologically relevant pH (pH 4, pH 6, pH 7.4), similarly to other NP dissolution studies.[26-29] Different siloxane precursors were employed during the core formation in order to produce

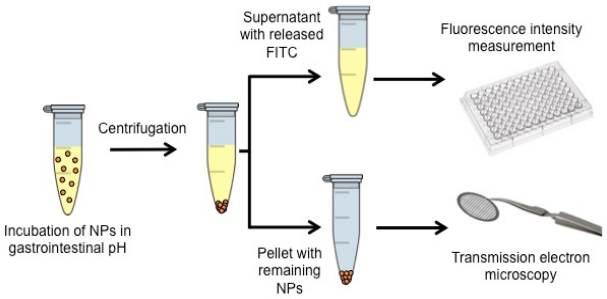

Figure 2: NPs were synthesised using tetraethoxysilane (NP_{TEOS}), ethyl triethoxysilane (NP_{ETOS}) or equal ratio of both ($NP_{50\text{-}50}$), and were degraded in biologically relevant pH . Dissolution of the NPs was assessed by fluorimetry (FITC release from the NPs) and electron microscopy (NP morphology and integrity).

particles that exhibit varying degrees of hydrophobicity, which in turn may be able to affect NP dissolution and the ability to host different cargos. A shell composed of tetraethoxysilane (TEOS) and negatively charged phosphonates was then added to each set of particles to insure similar surface chemistry.

The precursors used for core formation were TEOS, ethyl triethoxysilane (ETOS), bis(triethoxysilyl)benzene and bis(triethoxsilyl)biphenyl. However, the colloids formed using the aromatic oxysilanes were unstable in aqueous conditions and only particles formed using TEOS and ETOS were studied to assess dissolution. Degradation and release of the encapsulated cargo (i.e. fluorescein; FITC) from the SiNPs were monitored by electron microscopy and fluorimetry (Figure 2), and stability studies were carried out using dynamic light scattering (DLS). Overall, negligible dissolution was observed at pH 4 and suggested the NPs may survive the acidic conditions of the stomach or cellular lysosome, thus minimising cargo release. NP degradation was accelerated in pH 6 and pH 7.4 and may support the release the encapsulated cargo in small intestinal pH, at physiological pH or in early endosomes. A study mimicking progress through the GI tract (i.e. pH 4 to pH6 to pH 7.4) then showed the NPs released fluorescein in a pH-dependent manner, with NPs formed using more ETOS exhibiting 'burst' release profiles and those formed solely using TEOS displaying 'slow' release.

Methods

NPs synthesis and characterisation: materials, procedures, size and ζ-potential analysis, TEM studying of NP dissolution are detailed in the Supporting Information

FITC-release assay: The degree of FITC release was evaluated by measuring the amount of dye present in the supernatant and comparing the values measured with the fluorescent-based calibration curve for FITC at the corresponding pH. The values achieved from the independent experiments are reported as average (n = 3) ± SD. A Tecan Infinite M200 Pro Safire microplate reader was used for absorbance and fluorescence emission measurements. Samples were added to Nunc Maxisorb 96 well plates before being read (490/525 nm, $\lambda_{ex}/\lambda_{em}$). 250 µg of NP_{TEOS}, $NP_{50\text{-}50}$ and NP_{ETOS} were washed once by centrifugation and re-dispersion in water before dispersion in 1 ml of each phosphate buffer (pH 4, 6 or 7.4). For each sample in each buffer, 7 samples were prepared, one for each timepoint (1, 2, 4, 6, 8, 10, 24hrs) and shaken at 37°C (600 rpm). After each incubation time, samples were centrifuged (14000rpm, 10 min) and 700µL of supernatant were removed and the remainder discarded. The pellet isolated after centrifugation was washed twice by centrifugation and re-dispersion in water, then used for TEM analysis.

GI tract-like assay: 200µg of NP_{TEOS}, $NP_{50\text{-}50}$ and NP_{ETOS} were washed once by centrifugation and re-dispersion in water before dispersion in 1 mL of phosphate buffer at pH 4. The samples were shaken at 37°C (600 rpm). After 2 hours the samples were centrifuged, 300µL of the supernatant was measured (λ_{ex}/λem, 490/525 nm, 100µL per well). The remaining NP suspensions were filled with 300µL of fresh buffer pH 4 and re-incubated. After 2hr the samples were centrifuged and the supernatants completely removed and used for the fluorescence analysis, while the pellets were re-dispersed in 1 mL of buffer at pH 6 and shaken at 37°C (600 rpm). After 2 hours, the samples were centrifuged and the supernatants completely removed and used for the fluorescence analysis, while the pellets were re-dispersed in 1mL of buffer pH 7.4 and shaken again. The samples were centrifuged every 2 hours, 300µL of the supernatant were used to fill three wells of a 96-well plate and the fluorescence was measured. The experiment was stopped after 12hrs.

Results and Discussion

Core-shell microporous SiNPs were synthesised via the reverse microemulsion method[30,31] and their dissolution in biologically relevant pH was investigated. Different organosiloxane precursors were employed during core formation to produce particles with varying degrees of hydrophobicity and core crosslinking densities. FITC was modified with aminopropyl trimethoxysilane via thiourea bond formation and enabled the dye to be covalently incorporated into the silica matrix during core formation alongside the SiNP precursors (Figure 1).[31,32] A shell composed of TEOS and negatively charged phosphonates was then added to each set of particles to insure similar surface chemistry.[33] From the organosiloxane analogues chosen for this study, tetraethoxysilane (TEOS), the traditional SiNP precursor, and ethyl triethoxysilane (ETOS) were the only analogues capable of forming colloids that were stable in aqueous conditions. These NPs have been named NP_{TEOS} and NP_{ETOS} respectively. TEOS and ETOS were also added to the microemulsion in equal molar ratios, thus yielding a third batch of NPs: $NP_{50\text{-}50}$.

Two other siloxanes, bis(triethoxsilyl)benzene and bis(triethoxsilyl)biphenyl, were also used alongside TEOS as precursors for NP core formation. It was possible to generate stable NPs in ethanol using both siloxanes but they visually aggregated in less than one minute when transferred to DI water (Figure S1). Their rapid aggregation was attributed to the hydrophobic nature of their aromatic moiety and their potential to π-stack in water, and suggests further surface chemical modification (such as by PEGylation) would be needed to increase solubility in biological conditions. Even NPs formed using a 95:5 TEOS:bis(triethoxsilyl)benzene visually aggregated in aqueous medium (Figure S2).

Table 1: Physiochemical characterisation of the NP_{TEOS}, $NP_{50\text{-}50}$ and NP_{ETOS} by DLS and TEM. FITC loading per NP was also quantified and allowed for percentage of FITC release to be determined in later dissolution experiments (n=3).

	DLS			TEM	Loading
	Z-Av. Ø (nm)	PDI	ζ-potential (mV)	Ø (nm)	FITC per NP
NP_{TEOS}	132.5 ± 1.3	0.177 ± 0.016	-27.8 ± 0.80	72 ± 8	1256 ± 389
$NP_{50\text{-}50}$	170.0 ± 2.2	0.147± 0.005	-24.0 ± 0.27	80 ± 13	1578 ± 574
NP_{ETOS}	222.9 ± 6.0	0.275 ± 0.030	-22.3 ± 0.65	50 ± 31	122 ± 27

The three NPs (NP_{TEOS}, $NP_{50\text{-}50}$ and NP_{ETOS}) were characterised by DLS and transmission electron microscopy (TEM) in order to quantify particle size and surface charge (Table 1). Using TEM, the NP diameters were measured to be 72±8 nm, 80±13 nm and 50±31 nm for NP_{TEOS}, $NP_{50\text{-}50}$ and NP_{ETOS} respectively. However, using DLS, the size (Z-average) of the NP_{TEOS}, $NP_{50\text{-}50}$ and NP_{ETOS} was 132.5±1.3 nm, 170.0±2.2 nm, 222.9±6.0 nm. The NP Z-average size increased with the increasing proportion of ETOS, which was accompanied by the decrease of the absolute values of overall negative charge for the three NPs: -27.8±0.80 mV, -24.0±0.27 mV, -22.3±0.65 mV for NP_{TEOS}, $NP_{50\text{-}50}$ and NP_{ETOS}. This inverted correlation suggested that the NPs became less colloidally stable and experienced some degree of aggregation when more the hydrophobic ETOS was used during NP synthesis. No dramatic aggregation over a period of 2 days was observed for the NP_{TEOS} and $NP_{50\text{-}50}$ at pH 4, pH 6 and pH 7.4 buffers, but at pH 4, the NP_{ETOS} diameter increased gradually to 1µm (Figure 3). This effect is not desirable for drug delivery systems as increased NP size reduces the overall surface area-to-volume ratio, which is detrimental to controlled drug release, significantly changes the size-dependent properties of the NPs and may affect NP-cell interactions. However, in the case of *in vivo* drug delivery this is unlikely to be problematic since, in the case of oral administration, the residence time of food in the stomach is typically 4 hours or less. For intracellular delivery, NPs are likely to be firstly administered intravenously before reaching a tumour site (i.e. at pH 7.4 where they are stable). NP localisation in organs usually only then takes a matter of hours, during which time they are endocytosed and eventually trafficked to late endosomes/ lysosomes (pH 4).

The dissolution of SiNPs is well described in the literature and is caused by hydrolysis of the silica matrix, which is accelerated at higher pH and temperature.[21,34] Park et al described the hollowing of SiNPs due to etching under basic conditions.[35]

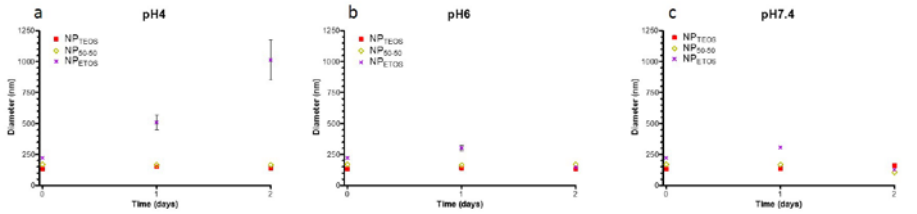

Figure 3: DLS analysis of NP size (Z-average, n=3) over a 2 day period in the pH 4, pH 6 and pH 7.4 buffers. (a) NP_{TEOS} and $NP_{50\text{-}50}$ were stable over time, but NP_{ETOS} gradually aggregated into micron-sized particles over 48 hours. (b) All NPs remained colloidally stable for 2 days at pH 6. (c) At pH7.4, the three sets of NPs also retained their colloidal stability for 2 days.

The authors suggested that small 'seed pores' in the particle matrix merge to form single voids and eventually results in large hollows. Mahon et al. demonstrated that SiNPs can degrade during *in vitro* cellular experimentation and observed NP hollowing by TEM following particle incubation in cell culture medium at 37°C.[34] We have also recently observed hollowing in a 'dissolution assay' designed to exploit SiNP degradation as a way to improve immunoassay signal-to-noise ratios.[21]

To this end, we have incubated NP_{TEOS}, $NP_{50\text{-}50}$ and NP_{ETOS} in buffered solutions at pH 4, pH 6 and pH 7.4 and analysed the NP integrity (i.e. the presence/absence of cavities/hollows) as an indicator of degradation. Clear changes in NPs morphology were observed after 6 hours at 37°C (Figure 4), and a complete 24 hour degradation study by TEM is presented in the Supporting Information (Figure S3, S4, S5). It is evident from Figure 4 that no changes in particle morphology were found for NP_{TEOS}, $NP_{50\text{-}50}$ or NP_{ETOS} when incubated at pH4. Small mesopore-sized hollows only became visible at pH4 in NP_{TEOS} after 24 hours of incubation (Figure S3, Table S3). This suggests that the three types of SiNPs would be robust enough to remain intact in the stomach ('fed state') and presumably also in the 'fasted state' (approx. pH 1.2)[36,37] because particle hydrolysis would be slower in more acidic conditions. However, the NPs would not be capable of intracellular dissolution-based cargo release if the colloids were eventually trafficked to lysosomes.

At pH 6, we noticed that degradation of the colloids had occurred in the NP_{TEOS} and $NP_{50\text{-}50}$, but was not evident in the NP_{ETOS} particles. For the $NP_{50\text{-}50}$ samples, clear mesopore-scale hollows measuring 13.71±4.93 nm in diameter in the could be seen after 2 hours and was further evidenced by the micrographs taken from 6 to 24 hours in which the etching is seen to be further enhanced (Fig S4, Table 3). NP_{TEOS} did not exhibit visible degradation at 2 hours at pH 6 but 6.96±3.73 nm hollows were clearly evident after 6 hours. Such hollowed structures are consistent with those found in other studies focussed on SiNP degradation.[21,34,35] Interestingly NP_{ETOS} exhibited no visual hollowing in the NP core at pH 6, which is presumably a result of the hydrophobic ethyl groups reducing the presence of water in the silica matrix, thus inhibiting the hydrolysis of the –O-Si-O– bond. Interestingly, it appeared that NP_{ETOS} underwent a dissolution process that led to gradual disintegration of the exterior particle surface. The apparent method of NP_{ETOS} degradation is therefore different to that of NP_{TEOS} and $NP_{50\text{-}50}$, and is presumably linked to the hydrophobic/hydrophilic nature of the respective particle cores. It is possible that the more hydrophilic cores of NP_{TEOS} and $NP_{50\text{-}50}$ are susceptible to initial etching by hydrolysis and followed the 'seed pore' phenomenon[35] to eventually form mesoscopic cavities. On the other hand, the hydrophobic NP_{ETOS} core resisted hydrolysis and dissolution occurred at the particle exterior that was formed only by using TEOS.

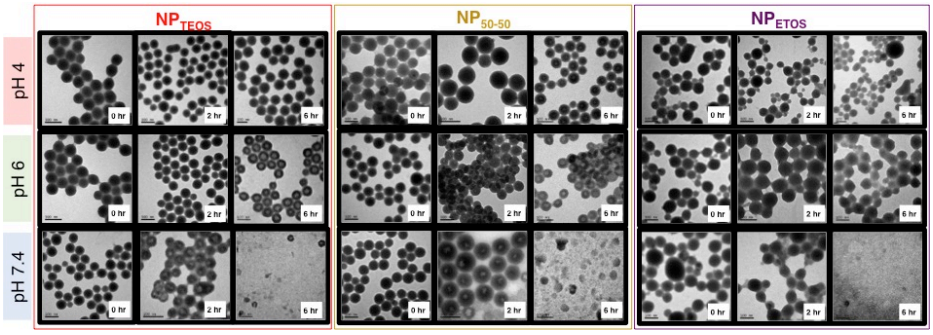

Figure 4: TEM of NP_{TEOS}, $NP_{50\text{-}50}$, and NP_{ETOS} incubated over time in pH 4, pH 6 and pH 7.4 solutions. No changes in NP morphology were observed in pH 4 over time which suggested silica NPs may be capable of enduring the harsh conditions of the stomach. NPs dissolved in pH 6 and pH7.4 due to the increased rate of hydrolysis of the silica matrix. Differences were observed in the mode of dissolution of NP_{TEOS} and $NP_{50\text{-}50}$ compared to NP_{ETOS}: Hollowing of the particle core was present in NP_{TEOS} and $NP_{50\text{-}50}$, whereas NP_{ETOS} degradation appeared to begin at the particle exterior surface.

Commented [G1]: I would say CLEAR hollow formation after 2 h…because, I know it is very hard to see, but there are some, not many, little hollow even after 1h. Otherwise thelate it from the table as well

Commented [CM2]: Is this an appropriate term?

A striking difference in NP integrity was found for particles incubated in pH 7.4 buffer. NP_{TEOS} and $NP_{50\text{-}50}$ exhibited more severe etching after 2 hours incubation compared to pH 6, which is in agreement with the hypothesis that increased basic conditions lead to more rapid silica hydrolysis and particle dissolution. Indeed, it is clear from the TEM images that NP_{TEOS} and $NP_{50\text{-}50}$ exhibited an evolution from a microporous structure to a hollowed mesoporous one, which can increase the overall NP surface area and further enhance degradation. This accelerated NP dissolution for both sets of NPs at pH 7.4 caused NP_{TEOS} and $NP_{50\text{-}50}$ to be largely degraded after 6 hours. TEM showed very few intact particles and features observed were predominantly NP debris, which agrees with previous SiNP degradation studies.[21] Further analysis of the NP hollows was conducted by scanning transmission electron microscopy (Figure S6). The results show that the hollowed interior the NPs could eventually etch through to the surface of NP_{TEOS} and $NP_{50\text{-}50}$ as a way of reducing surface energy,[35] and resulted in distinct surface deformations of the NPs.

The fact that NP_{TEOS}, $NP_{50\text{-}50}$ and NP_{ETOS} all degraded at pH7.4 is promising for oral drug delivery as the jejunum (pH 7.4) exhibits larger villi compared to do duodenum (pH 6). This means drugs released at this point in the GI tract would be readily absorbed, thus improving bioavailability before proceeding to enterohepatic circulation. Considering that the NP matrix almost completely disintegrates under these conditions, it may avoid any potential nanotoxicity issues and be cleared from the body. Indeed, silica is used in the food industry as a bulking agent in a number of food products (E551; silicium dioxide) and has been reported to degrade into biocompatible silicic acid.[38] However, dissolution of the NPs at pH 7.4 poses a challenge for intracellular delivery as this strategy first involves intravenous NP injection, which exposes the NPs to a pH 7.4 environment, and suggests some of the encapsulated cargo would diffuse from the nanomaterial before localisation. In turn, the total amount of drug transported across the cell membrane would be reduced.

Fluorescein isothiocyanate (FITC) was covalently bound inside the core of NP_{TEOS}, $NP_{50\text{-}50}$ and NP_{ETOS} and served as an indicator of NP degradation. The release profile of FITC into solution can therefore be used to infer the extent of NP dissolution and can be corroborated with the TEM images. Due to the hydrophobic nature of FITC (an analogue for poorly soluble drugs), monitoring the dye release also allowed for

concurrent assessment of the release profile of small molecules from the three sets of NPs over time. At each time point, the NPs were centrifuged and intact NPs were concentrated into a pellet, thus allowing the supernatant to be used for analysing free FITC released from the NPs (Figure 2). The quantity of dye released was then extrapolated from the calibration curves of known FITC concentrations prepared at the three different pHs in order to account for FITC's pH-dependent fluorescence emission intensity. The results of this FITC release study are presented in Figure 5.

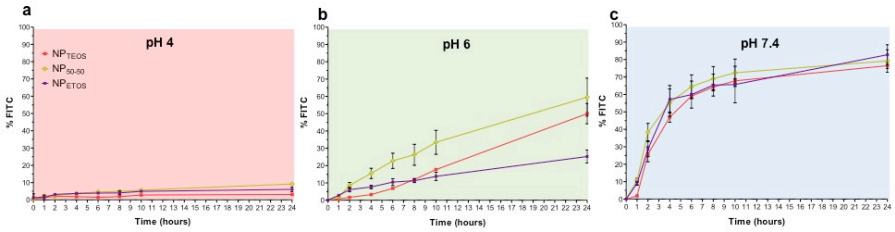

Figure 5: FITC release from the NPs over time when incubated in gastrointestinal pH's. (a) NPs were incubated in pH 4 solution and little FITC was detected in the sample supernatant over a 24 hour period. (b) In pH 6 gradual FITC release was observed and was attributed to increased hydrolysis rate compared to pH 4. (c) NP degradation was most rapid in pH 7.4 and release the majority of the FITC cargo into solution over time.

FITC release from NP_{TEOS}, $NP_{50\text{-}50}$ and NP_{ETOS} was minimal at pH 4 over the course of 24 hours (Figure 5a). The overall concentration of released FITC was less than 5% after 2 hours in the acidic environment and when considering the images of intact NPs obtained via TEM (Figure 4), it suggests that the SiNPs employed in this study would be capable of resisting degradation in the stomach. They may therefore be able to reliably carry drugs to the intestine, and agrees with other reports focussed on silica NP integrity in the stomach and the GI tract as a whole.[36,37] This was further supported by the fact that less than 10% of FITC was released from NP_{TEOS}, $NP_{50\text{-}50}$ and NP_{ETOS} at pH 4 after 24 hours. In addition, the low release rate of the dye into solution suggested SiNPs intracellularly trafficked to late endosomes/lysosomes would not release encapsulated cargo via NP dissolution and alternative strategies of ensuring drug delivery would be needed. For example, strategies like changes to NP shape or surface chemistry may ensure escape from intracellular vesicles into the more dissolution-friendly conditions of the cytosol (pH 7 - 7.4),[39-41] thus avoiding potential NP exocytosis.[42]

At pH 6, an increase in dye release was seen over time for the three NP formulations, although NP_{TEOS} releases FITC at a slower rate than both $NP_{50\text{-}50}$ and

NP_{ETOS} in the first 8 hours (Figure 5b). This is likely due to the more highly crosslinked nature of the core formed solely from TEOS, which results in slower dye diffusion out of NP_{TEOS}. Nonetheless, it is clear that increasing the pH from 4 to 6 led to more rapid dye release from the NPs and is attributed to the increased rate of hydrolysis at higher pH causing particle dissolution.

The fluorescence data of the NPs at pH 7.4 clearly showed that dye release due to NP degradation allowed for more rapid release of FITC (Figure 5c). This result correlated well with the electron microscopy results (Figure 2, S3, S4, S5 S6) from which it is evident that extensive particle dissolution occurred after 6 hours. More than 55% of FITC was released from NP_{TEOS}, $NP_{50\text{-}50}$ and NP_{ETOS} after 6 hours, which, in the case of oral drug delivery, suggested that small intestine would be the location where the majority of drugs would become available for absorption. This is clearly positive as this would lead to more efficacious delivery of the therapeutic. The loss of dye at pH 7.4 may not be beneficial for intracellular delivery as the cargo can be released before localising at tumour sites and prior to endocytosis. The fluorescence data also agrees with the findings of Mahon *et al.* where dye-leaching from SiNPs caused by NP dissolution can occur at physiological pH *in vitro*.[34] The authors then developed an alternative SiNP synthetic approach to prevent SiNP dissolution and dye-leaching in *in vitro* conditions.

Considering the favourable fluorescein retention in acidic conditions and release at higher pH, we decided to investigate whether the microporous SiNPs synthesised in this study may be suited to oral drug delivery. FITC release was monitored over time while increasing the pH, in an attempt to mimic the pH conditions of the whole GI tract and the digestion process (i.e. stomach, pH 4, to duodenum, pH6, to jejunum, pH 7.4, Figure 6a). The results are summarised in Figure 6b as free data points.

As expected, at pH 4 the NPs released less than 10% of the FITC cargo over a 4-hour period. However, when the pH increased to 6 a difference in dye release was observed for NP_{TEOS}, $NP_{50\text{-}50}$ and NP_{ETOS}. $NP_{50\text{-}50}$ release was higher than NP_{TEOS} and NP_{ETOS} at pH 6 solution. However, the most dramatic trend was the 'burst release' profile of FITC from NP_{ETOS} whilst incubated at pH 6 and pH 7.4. Only 3% of the FITC cargo was released at pH 4 over 4 hours, but once the NP_{ETOS} experienced small intestine-like conditions, the rate of release rapidly increased and 70% of dye was released into solution after 8 hours. The overall release of FITC from NP_{ETOS} was 80% after 12 hours. While $NP_{50\text{-}50}$ showed the highest release of FITC at pH 6, no dramatic increase in release was observed at pH 7.4, with 62% of the loaded FITC was detected in the

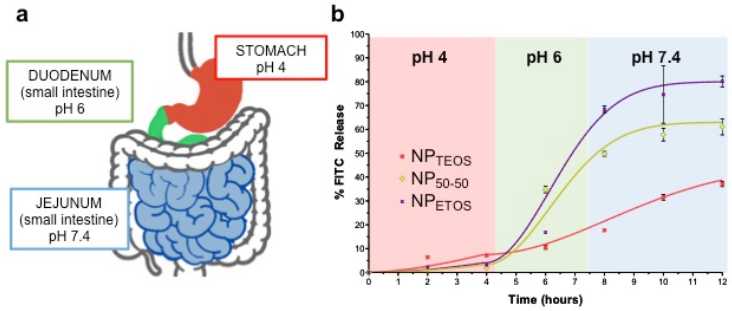

Figure 6: (a) The pathway through the gastrointestinal tract was mimicked over time. Stomach pH (pH 4) refers to that of 'fed state' and the requirement for some therapeutics like nonsteroidal anti-inflammatory drugs to be administered concurrently with food ingestion (b) Marginal FITC was released at pH4. Then, a pH-dependent dye release profile was observed for the respective NPs. NP_{TEOS} released FITC slowly and in a sustained manner at pH 6 and pH 7.4. $NP_{50\text{-}50}$ and NP_{ETOS} displayed initial burst release at pH 6 followed by a steady release at pH 7.4. Greater dye retention in the NPs was observed when increased TEOS was used for core formation. The free data points were used to manually fit Higuchi-Peppas models.

supernatant after 12 hours. On the other hand, NP_{TEOS} exhibited slow dye release at pH 6 and pH 7.4 and released less than 40% of its fluorescent cargo after 12 hours.

To further understand the FITC release from the NP_{TEOS}, $NP_{50\text{-}50}$ and NP_{ETOS} presented in Figure 6b, the Peppas kinetic model was considered as an appropriate model to assess diffusion-based cargo release from drug delivery systems.[43,44] The model is typically applied to polymeric systems (SI, Equations 1 and 2). The dye release was simulated for NP_{TEOS}, $NP_{50\text{-}50}$ and NP_{ETOS} and the simulated profiles appeared to fit the experimental observations well. The same rate constants were used for the fitting of the $NP_{50\text{-}50}$ and NP_{ETOS} data which suggests the incorporation of ETOS in the NP core led to similar dye diffusion pathways for the two types of colloid. However, the higher retention of FITC by $NP_{50\text{-}50}$ compared to NP_{ETOS} suggested that the former presumably

had a more densely formed silica matrix that eventually limited the release of the dye during the time period studied. Different rate constants were needed to fit the NP_{TEOS} data and suggested a different overall FITC release mechanism compared to both $NP_{50\text{-}50}$ and NP_{ETOS}. This is consistent with the hypothesis where a higher crosslinking density in a NP core matrix formed from TEOS alone and was reflected by the higher retention of FITC after 12 hours. The results presented in Figure 6b therefore show that increasing the amount of ETOS during NP synthesis would lead to increased cargo release at the pH found in small intestine (i.e. pH 6 and 7.4). This may prove beneficial if a 'burst release' profile is desirable, whereas it would be preferable to employ NPs formulated solely from TEOS for slower molecular release into the small intestine.

These findings established that SiNPs exhibit pH-dependent dissolution profiles, and it is possible to synthesise SiNPs that exhibit different cargo release profiles that hold potential in oral drug delivery applications. The ease at which these microporous NPs were synthesised and shown to exhibit different dissolution behaviour suggests that a number of further studies should be performed with encapsulated molecules of various physicochemical properties. We have also previously developed methodologies for extending SiNP storage and long-term stability, [22,45] and implied that the successful approaches for synthesising microporous SiNP with drug molecules could potentially be developed into realistic nano-delivery systems. In addition, the particles presented here may also be applicable to the emerging field of nano-nutraceuticals;[1,44,46] a field concerned with tuning molecule release kinetics and absorption using nano-sized carriers for more effective nutrient delivery systems. The use of microporous SiNPs therefore offers a number of potential routes for improved transport, protection and release of therapies in oral drug delivery and indeed the drug delivery field as a whole.

Conclusion

Microporous SiNPs with core-shell architecture were synthesised and their dissolution in biologically relevant pH (pH 4, pH 6, pH 7.4) was assessed. These pH refer to those found intracellularly and in the gastrointestinal tract. NP cores were formed using tetraethoxysilane (NP_{TEOS}), ethyl triethoxysilane (NP_{ETOS}) or a 1:1 ratio of both precursors ($NP_{50\text{-}50}$). These NPs did not degrade in pH 4 conditions but exhibited

degradation and fluorescein-release at pH 6 and pH 7.4. This was attributed to accelerated hydrolysis of the silica matrix at higher pH, the formation of mesopore-sized hollows and subsequent NP dissolution. This suggested that dissolution-based cargo release from the NPs presented here may be more likely to diffuse from of the NPs at physiological pH (pH 7.4) before being endocytosed and entering intracellular vesicles (pH 6 – early endosome, pH 4 - late endosome/lysosome). The degradation of the NPs at pH 7.4 also infers that this class of nanomaterial could be safely cleared and excreted. On the other hand, the retention of the fluorescein cargo in acidic conditions meant the NPs could be applicable to oral drug delivery where drugs required protection in the stomach. In a mimicked gastrointestinal tract study, increasing the amount of ETOS in the NP core formation led to increased release of FITC in pH 6 and pH 7.4 solutions. The release profiles of FITC are consistent with the hypothesis that cargo release from the NPs is controlled in part by the crosslinking density of the silica core, with ETOS generating a less dense matrix that facilitates greater cargo release at small intestinal pH (pH 6 and pH 7.4). The data obtained for NP_{TEOS} suggests this class of SiNP would be more suited to slow drug release in oral drug delivery applications. Overall, while further studies are needed to elucidate the degradation mechanisms associated with the colloidal systems presented here, we showed that it was possible to tune the release of encapsulated from SiNPs by simply changing the precursor used during NP synthesis. Microporous SiNPs therefore hold potential as a flexible platform upon which to base oral drug delivery strategies.

Acknowledgements: GG thanks the University of Kent for the provision of her PhD scholarship

References

1 J. Gleeson, S. Ryan and D. Brayden, *Trends in Food Science & Technology,* 2016, **53**, 90-101 (DOI:10.1016/j.tifs.2016.05.007).

2 A. Tivnan, W. Orr, V. Gubala, R. Nooney, D. Williams, C. McDonagh, S. Prenter, H. Harvey, R. Domingo-Fernandez, I. Bray, O. Piskareva, C. Ng, H. Lode, A. Davidoff and R. Stallings, *PLoS One,* 2012, **7**, e38129 (DOI:10.1371/journal.pone.0038129).

3 L. Chuah, C. Roberts, N. Billa, S. Abdullah and R. Rosli, *Coll. Surf B Biointerfaces,* 2014, **116**, 228-236 (DOI:10.1016/j.colsurfb.2014.01.007).

4 H. Amekyeh, N. Billa and C. Roberts, *Int. J. Pharm.,* **517**, 42-49 (DOI:10.1016/j.ijpharm.2016.12.001).

5 C. Lien, É Molnaŕ, P. Toman, J. Tsibouklis, G. Pilkington, D. Goŕecki and E. Barbu, *Biomacromolecules,* 2012, **13**, 1067-1073 (DOI:10.1021/bm201790s).

6 C. Saraiva, C. Praça, R. Ferreira, T. Santos, L. Ferreira and L. Bernardino, *J. Contr. Rel.,* 2016, **235**, 34-47 (DOI:10.1016/j.jconrel.2016.05.044).

7 F. Barandeh, P. Nguyen, R. Kumar, G. Iacobucci, M. Kuznicki, A. Kosterman, E. Bergey, P. Prasad and S. Gunawardena, *PLoS One,* 2012, **7**, e29424 (DOI:10.1371/journal.pone.0029424).

8 J. Florek, R. Caillard and F. Kleitz, *Nanoscale,* 2017, **9**, 15252-15277 (DOI:10.1039/C7NR05762H).

9 E. Phillips, O. Penate-Medina, P. Zanzonico, R. Carvajal, P. Mohan, Y. Ye, J. Humm, M. Gönen, S. Kalaigian H., H. Strauss, S. Larson, U. Wiesner and M. Bradbury, *Sci. Trans. Med,* 2014, **6**, 260ra149 (DOI:10.1126/scitranslmed.3009524).

10 Y. Yang, Z. Song, B. Cheng, K. Xiang, X. Chen, J. Liu, A. Cao, Y. Wang, Y. Liu and H. Wang, *J. Applied Toxicology,* 2013, **34**, 424-435 (DOI:10.1002/jat.2962).

11 R. Guillet-Nicolas, A. Popat, J. Bridot, G. Monteith, S. Qiao and F. Kleitz, *Angew. Chem. Int. Ed.,* 2013, **52**, 2318-2322 (DOI:10.1002/anie.201208840).

12 L. Li, T. Liu, C. Fu, L. Tan, X. Meng and H. Liu, *Nanomedicine: Nanotechnology, Biology and Medicine,* 2015, **11**, 1915-1924 (DOI:10.1016/j.nano.2015.07.004).

13 A. Popat, S. Jambhrunkar, J. Zhang, J. Yang, H. Zhang, A. Meka and C. Yu, *Chem. Comm.,* 2014, **50**, 5547-5550 (DOI:10.1039/C4CC00620H).

14 Z. Li, J. Barnes, A. Bosoy, J. Stoddart and J. Zink, *Chem. Soc. Rev.,* 2012, **41**, 2590-2605 (DOI:10.1039/C1CS15246G).

15 L. McCusker, F. Liebau and G. Engelhardt, *Pure Appl. Chem.,* 2001, **73**, 381-394.

16 M. Thommes, K. Kaneko, A. Neimark, J. Olivier, F. Rodriguez-Reinoso, J. Rouquerol and K. Sing, *Pure Appl. Chem.,* 2015, **87**, 1051-1069 (DOI:10.1515/pac-2014-1117).

17 T. Ohulchanskyy, I. Roy, L. Goswami, Y. Chen, E. Bergey, R. Pandey, A. Oseroff and P. Prasad, *Nano Lett.,* 2007, **7**, 2835-2842 (DOI:10.1021/nl0714637).

18 B. Riva, M. Bellini, E. Corvi, P. Verderio, E. Rozek, B. Colzani, S. Avvakumova, A. Radeghieri, M. Rizzuto, C. Morasso, M. Colombo and D. Prosperi, *J. Coll. Interface Sci.,* 2018, **519**, 18-26 (DOI:10.1016/j.jcis.2018.02.040).

19 L. Tang and J. Cheng, *Nanotoday,* 2013, **8**, 290-312 (DOI:10.1016/j.nantod.2013.04.007).

20 R. Nooney, A. White, C. O'Mahony, C. O'Connell, K. Kelleher, S. Daniels and C. McDonagh, *J. Coll. Interface Sci.,* 2015, **456**, 50-58 (DOI:10.1016/j.jcis.2015.05.051).

21 C. Moore, G. Giovannini, F. Kunc, A. Hall and V. Gubala, *J. Mater. Chem. B,* 2017, **5**, 5564-5572 (DOI:10.1039/C7TB01284E).

22 C. Moore, H. Montón, R. O'Kennedy, D. Williams, C. Nogués, C. Crean (neé Lynam) and V. Gubala, *J. Mater Chem. B,* 2015, **3**, 2043-2055 (DOI:10.1039/C4TB01915F).

23 M. Benezra, O. Penate-Medina, P. Zanzonico, D. Schaer, H. Ow, A. Burns, E. DeStanchina, V. Longo, E. Herz, S. Iyer, J. Wolchok, S. Larson, U. Wiesner and M. Bradbury, *J. Clin. Invest.,* 2011, **121**, 2768-2780 (DOI:10.1172/JCI45600).

24 J. Fuller, G. Zugates, L. Ferreira, H. Ow, N. Nguyen, U. Wiesner and R. Langer, *Biomaterials,* 2012, **29**, 1526-1532 (DOI:10.1016/j.biomaterials.2007.11.025).

25 M. Ruedas-Rama, J. Walters, A. Orte and E. Hall, *Analytica Chimica Acta,* 2012, **751**, 1-23 (DOI:10.1016/j.aca.2012.09.025).

26 F. Aureli, M. D'Amato, B. De Berardis, A. Raggi, A. Turcoa and F. Cubadda, *J. Anal. At. Spectrom.,* 2012, **27**, 1540-1548 (DOI:10.1039/C2JA30133D).

27 E. Choi and S. Kim, *Langmuir,* 2017, **20**, 4974-4980 (DOI:10.1021/acs.langmuir.7b00332).

28 N. Summerlin, Z. Qua, N. Pujara, Y. Sheng, S. Jambhrunkar, M. McGuckin and A. Popat, *Coll. Surf. B,* 2016, **144**, 1-7 (DOI:10.1016/j.colsurfb.2016.03.076).

29 H. Yamada, C. Urata, Y. Aoyama, S. Osada, Y. Yamauchi and K. Kuroda, *Chem. Mater.,* 2012, **24**, 1462-1471 (DOI:10.1021/cm3001688).

30 R. Bagwe, C. Yang, L. Hilliard and W. Tan, *Langmuir,* 2004, **20**, 8336-8342 (DOI:10.1021/la049137j).

31 R. Nooney, E. McCormack and C. McDonagh, *Anal. Bioanal. Chem,* 2012, **404**, 2807-2818 (DOI:doi: 10.1007/s00216-012-6224-z).

32 A. Van Blaaderen and A. Vrij, *Langmuir,* 1992, **8**, 2921-2931 (DOI:10.1021/la00048a013).

33 R. Bagwe, L. Hilliard and W. Tan, *Langmuir,* 2006, **22**, 4357-4362 (DOI:10.1021/la052797j).

34 E. Mahon, D. Hristov and K. Dawson, *Chem. Commun.,* 2012, **48**, 7970-7972 (DOI:10.1039/C2CC34023B).

35 S. Park, Y. Kim and S. Park, *Langmuir,* 2008, **24**, 12134-12137 (DOI:10.1021/la8028885).

36 C. Fruijtier-Pölloth, *Archives of Toxicology,* 2016, **90**, 2885-2916 (DOI:10.1007/s00204-016-1850-4).

37 H. Winkler, M. Suter and H. Naegel, *Journal of Nanobiotechnology,* 2016, **14**, 44 (DOI:10.1186/s12951-016-0189-6).

38 J. Park, L. Gu, G. von Maltzahn, E. Ruoslahti, S. Bhatia and M. Sailor, *Nat. Mater.,* 2009, **8**, 331-336 (DOI:10.1038/nmat2398).

39 Z. Chu, S. Zhang, B. Zhang, C. Zhang, C. Fang, I. Rehor, P. Cigler, H. Chang, G. Lin, R. Liu and Q. Li, *Scientific Reports,* 2014, **4**, 4495 (DOI:10.1038/srep04495).

40 Z. Chu, K. Miu, P. Lung, S. Zhang, S. Zhao, H. Chang, G. Lin and Q. Li, *Scientific Reports,* 2015, **5**, 11661 (DOI:10.1038/srep11661).

41 E. Lukianova-Hleb, A. Belyanin, S. Kashinath, X. Wu and D. Lapotko, *Biomaterials,* 2012, **33**, 1821-1826 (DOI:10.1016/j.biomaterials.2011.11.015).

42 R. Yanes, D. Tarn, A. Hwang, D. Ferris, S. Sherman, C. Thomas, J. Lu, A. Pyle, J. Zink and F. Tamanoi, *Small,* 2013, **9**, 697-704 (DOI:10.1002/smll.201201811).

43 J. Siepmann and N. Peppas, *Int. J. Pharm.,* 2011, **418**, 6-12 (DOI:10.1016/j.ijpharm.2011.03.051).

44 M. Danish, G. Vozza, H. Byrne, J. Frias and S. Ryan, *Innovative Food Science and Emerging Technologies,* 2017, (DOI:10.1016/j.ifset.2017.07.002).

45 G. Giovannini, F. Kunc, C. Piras, O. Stranik, A. Edwards, A. Hall and V. Gubala, *RSC Adv.,* 2017, **7**, 19924-19933 (DOI:10.1039/C7RA02427D).

46 M. Danish, G. Vozza, H. Byrne, J. Frias and S. Ryan, *J. Food Science,* 2017, (DOI:10.1111/1750-3841.13824).

Supporting Information

pH-Dependent Silica Nanoparticle Dissolution and Cargo Release

Giorgia Giovaninni,[a] Colin J. Moore,[b*] Andrew J. Hall, [a] Hugh J. Byrne,[b] Vladimir Gubala [a]

[a]Medway School of Pharmacy, University of Kent, Central Ave, Chatham Maritime, Kent, ME4 4TB, United Kingdom

[b]FOCAS Research Institute, Dublin Institute of Technology, Kevin St., Dublin 8, Ireland

Email: gg238@kent.ac.uk, colin.moore@dit.ie, a.hall@kent.ac.uk, hugh.byrne@dit.ie, v.gubala@kent.ac.uk

*Corresponding author: colin.moore@dit.ie , Tel: +353 1 4027902 , Fax: +353 1 4027901

Additional experimental information

Materials

Cyclohexane (anhydrous, 99.5%), 1-hexanol (anhydrous, 99%), Triton® X-100, aminopropyl trimethoxysilane [APTMS] (97%), tetraethoxysilane[TEOS] (99.99%), ethyltriethoxysilane (96%)[ETOS], 4,4'-Bis(triethoxysilyl)biphenyl (95%) [bis(TE)PP], 4,4'-Bis(triethoxysilyl)benzene (96%) [bis(TE)B], ammonium hydroxide solution (28% w/v in water, ≥99.99%), 3-(trihydroxysilyl)propyl methylphosphonate monosodium salt (42% w/v in water) [THPMP], fluorescein isothiocyanate isomer I (≥90%)[FITC], sodium phosphate dibasic (>98.5%), sodium phosphate monobasic (>98%), sodium carbonate (≥99.5%), sodium bicarbonate (≥99.5%), were purchased from Sigma Aldrich. Sodium

carbonate (0.1M) combined with sodium bicarbonate (0.1M) yielded pH10.6 (9:1 v/v respectively) solutions. Absolute ethanol, transparent Nunc Maxisorb 96 well plates were purchased from Fisher Scientific. Carbon Films on 400 Mesh Grids Copper were purchased from Agar Scientific.

Nanoparticle synthesis

Dye precursor formation: In a dried glass vial, FITC (2.5 mg) was dissolved in 1-hexanol (2mL) with APTMS (5.6 µL). The reaction was stirred for 2 hours under a nitrogen atmosphere.

All nanoparticles were formed in a microemulsion prepared by combining cyclohehexane (7.5 mL), 1-hexanol (1.133 mL), Triton® X-100 (1.894 g) and DI water (0.48 mL) in a 30 mL plastic bottle under constant stirring. For the formation of the silica core, TEOS and ETOS were added in different ratios with quantity of oxysilane being equal 0,45 mmol.

	TEOS % (µL)	ETOS % (µL)
NP_{TEOS}	100% (100)	/
$NP_{50\text{-}50}$	50% (50)	50% (48)
NP_{ETOS}	/	100% (97)

Dye precursor solution (0.162 mL) was then added. After 30 minutes, 40 µL of ammonium hydroxide was added to trigger polymerisation. The mixture was stirred for further 24 hours. Nanoparticle shells were synthesised by adding 50 µL of TEOS. 20

minutes later 40 µL THPMP was added. After 5 minutes, 10 µL of APTMS was then added, and the mixture was allowed to stir at RT for another 24hrs. The microemulsion was then broken by adding 30 mL ethanol. Formed SiNPs were purified by centrifugation (14000 rpm, 10 min) and re-dispersion in ethanol (x3). After purification, the NPs were stored in ethanol at 4°C.

Quantification of FITC loading

In order to quantify the amount of FITC loaded during the synthetic procedure, 200 µg of each type of SiNPs were shaken (600 rpm) at 37°C in sodium carbonate/sodium bicarbonate (1:9) buffer at pH10.6 as previously reported.[21] After 5 hours, the samples were centrifuged (14000 rpm, 10 min) and no pellet was observed, meaning that the particles had dissolved. Three wells of the 96-well plate were filled with 200 µL of the supernatant isolated after centrifugation. The signal given by FITC molecules free in solution was compared to a fluorescence/absorbance-based calibration curve of known concentrations of FITC at pH10.6. The amount of dye loaded in 200 µg of particle were calculated. From the values obtained, the number of molecules per NP was calculated by using the spherical volume of the silica NPs calculated from average TEM diameters. The signal was read at 490/525 nm ($\lambda_{ex}/\lambda_{em}$). Values are reported as average of three independent batches of particles (n=3) ± SD.

Synthesis of NPs using benzene-oxysilanes

The same microemulsion and FITC-loading setup as described above was used except for the choice of oxysilanes. Again, a total of 0.45mmol of oxysilane was used. TEOS was used for NP formation alongside either bis(triethoxsilyl)benzene [bis(TE)B] or bis(triethoxsilyl)biphenyl [bis(TE)PP].

TEOS:Bis(TE) B	TEOS [µL]	Bis(TE)B [µL]
95:5	95	8.92
90:10	90	17.85
85:15	85	26.77
75:25	75	44.62
50:50	50	89.24
TEOS:Bis(TE) PP	TEOS [µL]	Bis(TE)PP [µL]
75:25	75	51.44
50:50	50	102.88

Nanoparticle shells were synthesised by adding 50 µL of TEOS, followed by 40 µL of THPMP and 10 µL of APTMS after 20min and 5min between each other. After 24h, the microemulsion was broken by adding 30 mL ethanol. Formed SiNPs were purified by centrifugation (14000 rpm, 10 min) and re-dispersion in ethanol (3x). After purification, the nanoparticles were stored in ethanol at 4°C.

Buffer preparation

Phosphate buffer at different pH were prepared mixing 0.2 M sodium phosphate dibasic and 0.2 M sodium phosphate monobasic and adjusting the pH to 4, 6 and 7.4 using 5 M NaOH and 5 M of HCl.

NP characterization

Dynamic light scattering and zetametry: SiNPs were dispersed at a concentration of 500µg/mL in DI water. Their size and zeta-potential were analysed in a disposable folded capillary cell (DTS1070) at RT using Malvern Zetasizer. n = 3, average ± SD.

SiNP stability: 250µg/mL of NP_{TEOS}, $NP_{50\text{-}50}$ and NP_{ETOS} were isolated and re-dispersed in 1mL of each buffer (pH 4, 6 and 7.4) and incubated at 37°C. Size and zeta potential were measured by DLS at 0hr, 24hr, 48hr using Malvern Zetasizer. n = 3, average ± SD.

Transmission electron microscopy: NP size quantification following synthesis: 5µL of NPs in water (500µg/mL) was added on 'Carbon Films on 400 Mesh Grids Copper' (Agar Scientific) and allowed to evaporate. Using ImageJ software, at least 100 NPs per image were analysed for NP diameter.

SiNPs dissolution using TEM: Following incubation in pH 4, 6, or 7.4 over different times, NP pellets were isolated using centrifugation (x3), washed using DI water in order to remove residues salts. The pellet was finally re-dispersed in 200µL DI water, 3µL added to 'Carbon Films on 400 Mesh Grids Copper' (Agar Scientific) and allowed to evaporate. Images were taken on a Joel JEM-3200FS at ×250, ×200, ×150 and ×100 magnification.

Scanning Transmission Electron Microscopy (STEM): SiNPs dissolution: The same grids as 'SiNPs dissolution using TEM' prepared for TEM analysis for the main text were used for STEM. The grids were analysed in STEM imaging mode using a Hitachi SU-6600 microscope. Images were taken in secondary electron (SE) and transmission electron (TE) mode at 130,000 magnification using either 20kV or 25kV accelerating voltage. The working distance was 8mm.

Data fitting of with Peppas model for data points in Figure 6b

The data from the release profile of the 'GI tract-like assay' was manually simulated with SigmaPlot using the diffusive models presented by Siepmann and Peppas. [43] Equation 1 was used to fit data from 0 to 4 hours.

$$\frac{M_t}{M_\infty} = (ks_1)\left(\sqrt{time}\right) + (ks_2)(time)$$

[Eq. 1]

where M_t is the diffused mass at a given time, M_∞ is the asymptotic diffused mass at infinite time, ks_1 and ks_2 are diffusive and relaxation constants. Equation 2 was used to fit the data from 4 to 12 hours.

$$\frac{M_t}{M_\infty} - \frac{M_4}{M_\infty} = (ki_1)\left(\sqrt{time - 4}\right) + (ki_2)(time - 4)$$

[Eq. 2]

where M_4 is the predicted diffused mass at the time of changing from pH4 to pH6 (i.e. after 4 hours). The rate constants used to for Equation 1 and 2 are presented below. M_∞ for NP_{TEOS}, $NP_{50\text{-}50}$ and NP_{ETOS} were 45, 63 and 80 respectively.

	NP_{TEOS}	**$NP_{50\text{-}50}$**	**NP_{ETOS}**
ks_1	0.02	0.0025	0.0025
ks_2	0.01	0.005	0.005
ki_1	0.01	0.001	0.001
ki_2	0.05	0.2	0.2

653 **Supporting Figures**

654

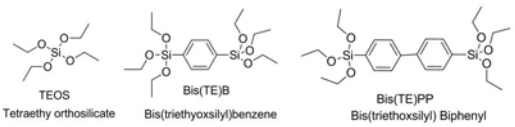

In ethanol		Z-average (nm)	Zeta Potential (mV)
TEOS : Bis(TE)B	75:25	170.1 ± 12.0	-20.6 ± 1.6
	50:50	177.3 ± 8.4	-29.8 ± 2.4
TEOS : Bis(TE)PP	75:25	179.7 ± 16.2	-5.8 ± 0.3
	50:50	180.7 ± 8.7	-9.3 ± 0.5

Rapid visual aggregation in DI water in less than 1 minute.

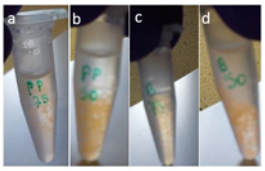

*Figure S1: FITC-doped silica NPs were formed by combining the traditional precursor TEOS and either bis(triethoxsilyl)benzene, Bis(TE)B, or bis(triethoxsilyl)biphenyl, Bis(TE)PP. The ratio TEOS:Bis(TE)B and TEOS:Bis(TE)PP was 75:25 and 50:50. The resultant colloids were soluble in ethanol and dynamic light scattering was used to quantify the diameter and zeta potential of the NPs (n=3), as shown in the above table. However, when they were dispersed in DI water the NPs visually aggregated in less than 1 minute. [**a** , **b**: TEOS:Bis(TE)B 75:25, 50:50]; **c, d**: TEOS:Bis(TE)PP]*

655

656

657

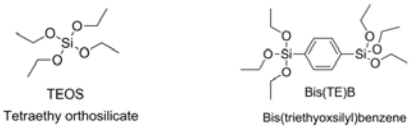

In water		Z-average (nm)		Zeta Potential (mV)	
		0 hours	24 hours	0 hours	24 hours
TEOS:Bis(TE)B	95:5	109.4 ± 3.8	97.7 ± 3.1	-32.1 ± 0.7	-31.9 ± 0.4
	90:10	114.5 ± 4.6	107.4 ± 4.8	-37.6 ± 1.2	-22.1 ± 3.1
	85:15	233.4 ± 19.6	231.0 ± 20.2	-31.1 ± 1.1	-14.1 ± 0.5

Visual aggregation in phosphate buffer saline in less than 10 minutes.

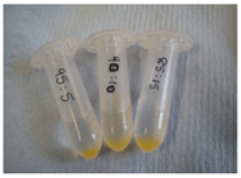

Figure S2: Bis(TE)B was incorporated in to FITC-loaded silica NPs in lower molar concentrations as a way make the resultant NPs 'less hydrophobic' and therefore stable in aqueous conditions. TEOS:Bis(TE)B was added to the microemulsion in 95:5, 90:10, 85:15 and were colloidally stable in DI water for 24 hours. However when the NPs were dispersed in PBS they visually aggregated after only 10 minutes.

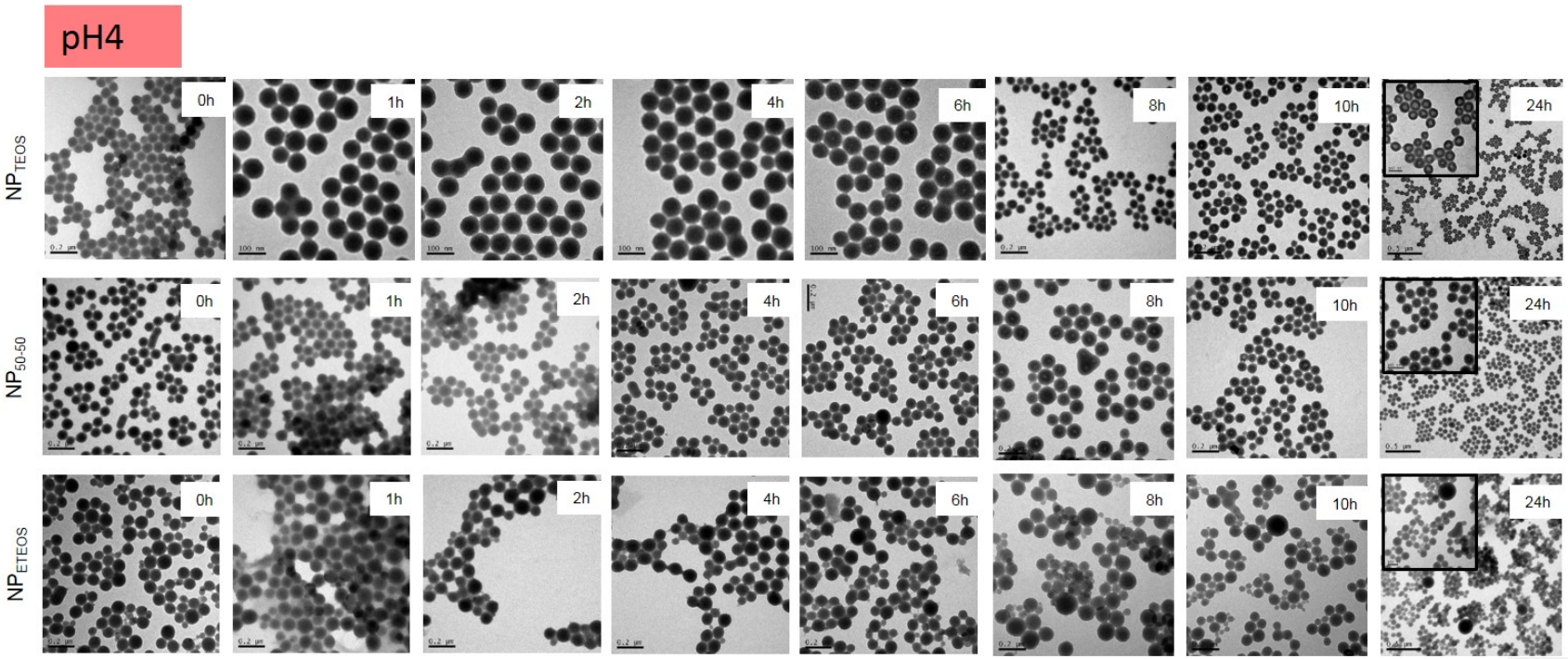

Figure S3: The three sets of NPs appeared in tact when incubated over time in pH 4

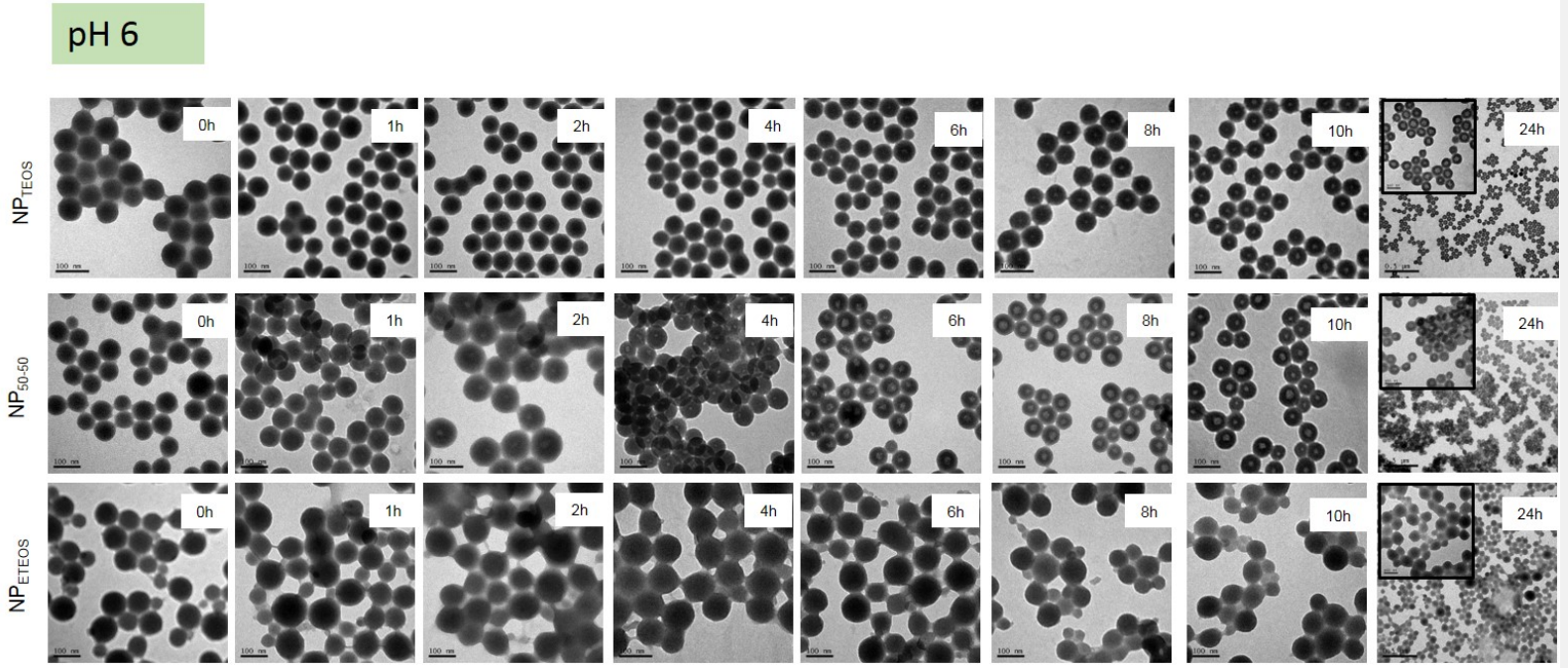

Figure S4: Degradation was visible by TEM for the three sets of NPs in pH 6 solution over time. Hollowing in the interior of NP_{TEOS} and $NP_{50\text{-}50}$ was observed after 6 – 8 hours whereas NP_{ETOS} appeared to degrade at the particle surface.

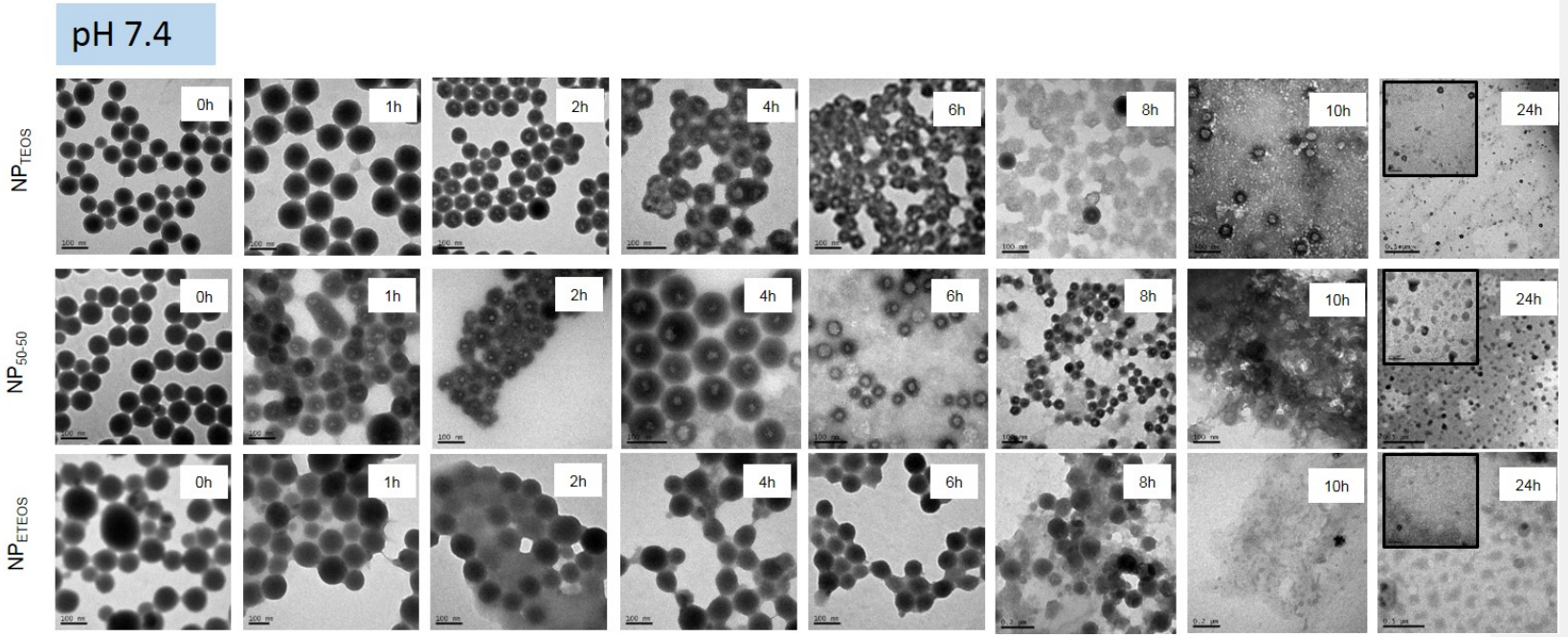

Figure S5: Degradation was visible by TEM for the three sets of NPs in pH 7.4 solution over time. More rapid hollowing of the interior of NP_{TEOS} and $NP_{50\text{-}50}$ was observed compared to those observed at pH 6. After 6 – 8 hours few NPs could be isolated after centrifugation and those after that time. NP_{ETOS} appeared to degrade at the particle surface. After 10 hours virtually no NPs were visible by TEM, and structures resembling colloids were highly degraded and surrounded by dissolution debris.

Table S3: The size of the NP hollows (or pores) where measured by TEM analysis using the micrographs from Figures S3, S4 and S5.. NM (not measurable) indicates that the particles did not present any visible pores, while DISS (dissolved) indicates that no particles were identifiable on the TEM grid and were therefore considered to be dissolved. Values are shown as average ± SD (n=30 approximately).

		0h	1h	2h	4h	6h	8h	10h	24h
pH4	**NP_{TEOS}**	NM	NM	NM	NM	9.65±5.30	7.79±3.33	14.11±4.85	32.84±7.69
	$NP_{50\text{-}50}$	NM	NM	NM	NM	NM	14.98±6,79	12.77±5.65	11.41±4.25
	NP_{ETEOS}	NM	NM	NM	NM	NM	NM	NM	NM
pH6	**NP_{TEOS}**	NM	NM	NM	NM	6.96±3.73	8.07±2.63	11.46±3.37	34.01±8.66
	$NP_{50\text{-}50}$	NM	7.52±2.19	13.71±4.93	11.11±3.18	16.39±5.50	24.61±6.16	20.31±7.32	26.91±6.17
	NP_{ETEOS}	NM	NM	NM	NM	NM	NM	NM	NM
pH7.4	**NP_{TEOS}**	NM	NM	11.76±3.43	13.45±4.93	4.80±1.44	DISS.	DISS.	DISS.
	$NP_{50\text{-}50}$	NM	15.39±5.38	14.91±4.80	20.45±6.50	21.16±7.2	13.35±4.40	DISS.	DISS.
	NP_{ETEOS}	NM	NM	NM	NM	NM	NM	DISS.	DISS.

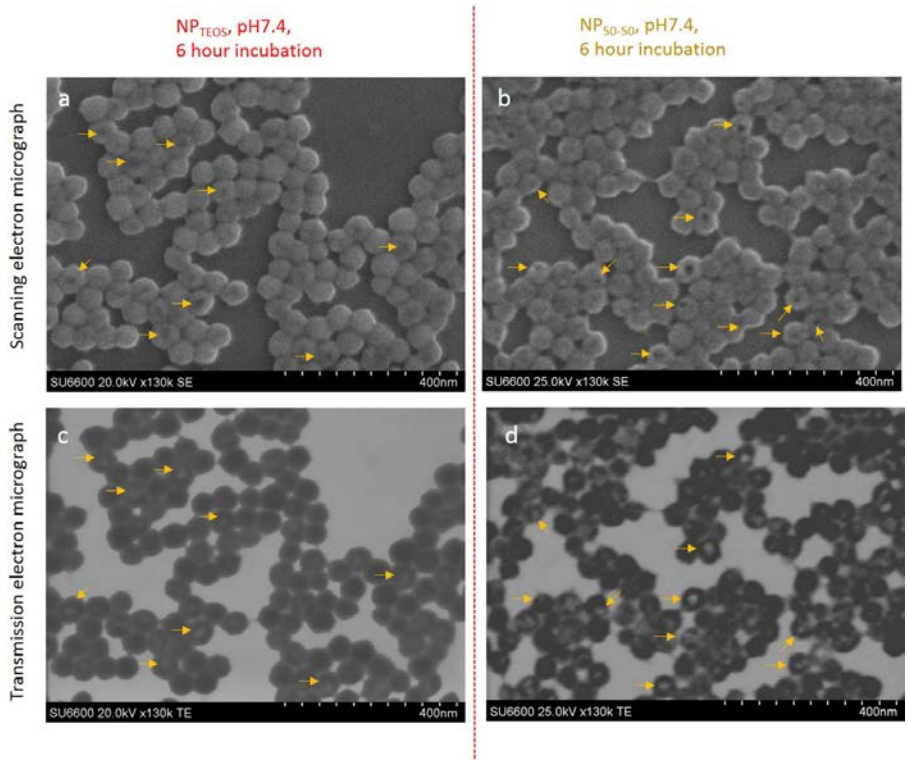

Figure S6: Scanning transmission electron microscopy allowed for secondary electrons (SE) to be obtained for scanning mode while transmission electrons (TE) could be detected simultaneously in transmission mode. ***(a,b)*** *Scanning electron micrographs showed that the surface deformations, highlighted by yellow arrows, were visualised as hollows in transmission electron micrographs* ***(c,d)****. It is therefore suggested to that studies investigating silica NP hollowing/etching of the core should also use scanning electron microscopy to interrogate the particle surface, thus providing a more accurate evaluation of the overall particle morphology and integrity.*